

Highlights

Efficient Neural Combinatorial Optimization Solver for the Min-max Heterogeneous Capacitated Vehicle Routing Problem

Xuan Wu, Di Wang, Chunguo Wu, Kaifang Qi, Chunyan Miao, Yubin Xiao, Jian Zhang, You Zhou

- We propose a dual-modality node encoder that jointly captures edge and node features.
- We explicitly emphasize the importance of the previously selected vehicle in guiding the current decoding decision.
- We propose a parameter-free cross attention mechanism to effectively incorporate features of the previously selected vehicle.
- We develop an efficient data augment method tailored for MMHCVRP with complex constraints.
- The proposed methods outperforms state-of-the-art methods across all evaluated settings.

Efficient Neural Combinatorial Optimization Solver for the Min-max Heterogeneous Capacitated Vehicle Routing Problem

Xuan Wu^a, Di Wang^b, Chunguo Wu^a, Kaifang Qi^c, Chunyan Miao^b, Yubin Xiao^{a,*}, Jian Zhang^{a,*}, You Zhou^{a,*}

^a*Key Laboratory of Symbolic Computation and Knowledge Engineering of Ministry of Education, College of Computer Science and Technology, Jilin University, Changchun, 130012, China*

^b*Joint NTU-UBC Research Centre of Excellence in Active Living for the Elderly, Nanyang Technological University, 639798, Singapore*

^c*College of Software, Jilin University, Changchun, 130012, China*

Abstract

Numerous Neural Combinatorial Optimization (NCO) solvers have been proposed to address Vehicle Routing Problems (VRPs). However, most of these solvers focus exclusively on single-vehicle VRP variants, overlooking the more realistic min-max Heterogeneous Capacitated Vehicle Routing Problem (MMHCVRP), which involves multiple vehicles. Existing MMHCVRP solvers typically select a vehicle and its next node to visit at each decoding step, but often make myopic decoding decisions and overlook key properties of MMHCVRP, including local topological relationships, vehicle permutation invariance, and node symmetry, resulting in suboptimal performance. To better address these limitations, we propose ECHO, an efficient NCO solver. First, ECHO exploits the proposed dual-modality node encoder to capture local topological relationships among nodes. Subsequently, to mitigate myopic decisions, ECHO employs the proposed Parameter-Free Cross-Attention mechanism to prioritize the vehicle selected in the preceding decoding step. Finally, leveraging vehicle permutation invariance and node symmetry, we introduce a tailored data augment strategy for MMHCVRP to stabilize the Reinforcement Learning training process. To assess the performance of ECHO, we conduct extensive experiments. The experimental results demonstrate

*Corresponding authors

that ECHO outperforms state-of-the-art NCO solvers across varying numbers of vehicles and nodes, and exhibits well-performing generalization across both scales and distribution patterns. Finally, ablation studies validate the effectiveness of all proposed methods.

Keywords: Neural Combinatorial Optimization, Heterogeneous Capacitated Vehicle Routing Problem, Deep Reinforcement Learning

1. Introduction

Vehicle Routing Problem (VRP) is a fundamental class of Combinatorial Optimization Problem (COP) with widespread applications in diverse domains, e.g., communication and transportation [1–5]. Conventional algorithms for solving VRPs can be broadly divided into three categories, namely exact, approximation, and heuristic algorithms [6–10]. However, these conventional algorithms cannot derive insights from historical VRP instances and lack the capability to solve multiple VRP instances in parallel, thus leading to significant computing overhead [11].

Recently, numerous Neural Combinatorial Optimization (NCO) solvers have been proposed to address the VRP [12–16]. These solvers can derive insights from historical instances and exploit GPU parallelism to process multiple VRP instances concurrently, achieving high-level performance with substantially reduced computational time [17, 18]. However, most existing NCO solvers focus on either the unconstrained Traveling Salesman Problem (TSP) or the Capacitated Vehicle Routing Problem (CVRP) with only basic capacity constraints [19, 20]. In practical applications, VRP variants often involve more complex attributes or constraints, thereby hindering the deployment of existing NCO research [21, 22]. For example, real-world scenarios frequently feature vehicles with heterogeneous attributes (e.g., capacity and speed), and fleet operators commonly aim to minimize the longest travel time among all vehicles (min-max) rather than the total time traveled by the entire fleet (min-sum). This problem is known as the min-max Heterogeneous Capacitated Vehicle Routing Problem (MMHCVRP).

Existing NCO methods for the MMHCVRP are typically trained via Reinforcement Learning (RL) and can be broadly categorized into two categories, namely AutoRegressive (AR) and Parallel-Autoregressive (PAR) solvers. AR-based solvers adopt an encoder-decoder architecture, where vehicle and node encoders embed vehicle and node features, respectively, and the decoder se-

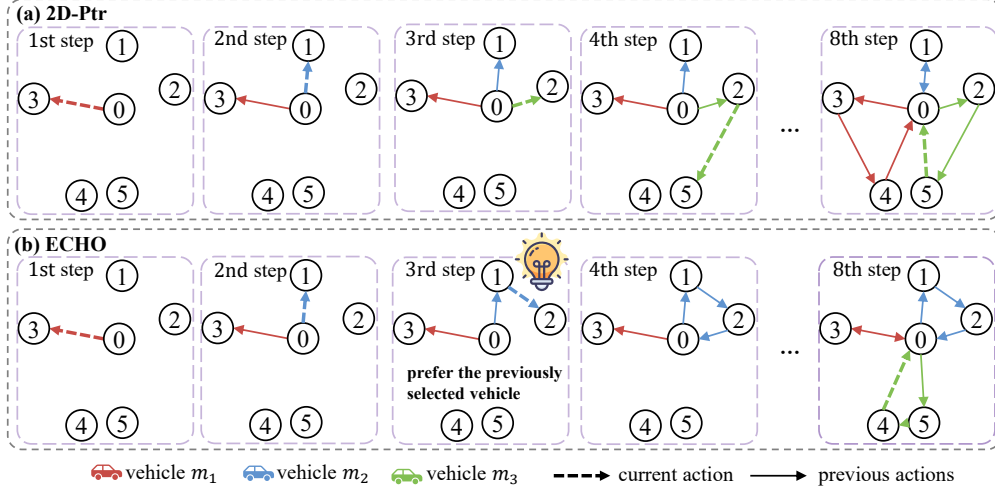


Figure 1: Illustration on the decoding processes of 2D-Ptr [23] (a) and the proposed ECHO (b). 2D-Ptr myopically relies on cumulative travel time to select the vehicle-node pair at each time step, which may lead to suboptimal solutions. Whereas the proposed ECHO alleviates this problem by emphasizing the vehicle selected in the preceding time step.

quentially selects a vehicle and its next node to visit at each time step [22, 23]. PAR-based solvers similarly employ the node and vehicle encoders to embed their respective features. However, during decoding, each vehicle simultaneously selects a node to visit at each time step. This parallel selection enables PAR-based solvers to perform inference faster than their AR-based counterparts. However, the resulting high-dimensional joint action space complicates training and may produce suboptimal solutions [24]. Moreover, conflicts arise when multiple vehicles simultaneously select the same node within a single time step. AR-based solvers also exhibit certain limitations. As shown in Fig. 1(a), these solvers disregard the priority of the vehicle selected in the preceding time step, relying solely on the accumulated travel time of each vehicle for decision-making. Consequently, at the third time step, vehicle m_3 is chosen to visit the node n_2 . While this short-sighted strategy may produce plausible solutions initially, it ultimately leads to suboptimal performance. Moreover, these solvers neglect key properties of the MMHCVRP, namely local topological relationships, vehicle permutation invariance, and node symmetry, which ultimately degrades their performance.

To better address these limitations, we propose an Efficient Neural Combinatorial Optimization Solver for the Min-max Heterogeneous Capacitated

Vehicle Routing Problem (**ECHO**). Specifically, to better capture local topological features, we replace the vanilla node encoder with our dual-modality node encoder, which employs a cross-attention mechanism to integrate node and edge features (see Section 4.1 for more details). This design endows ECHO with robust generalization capabilities across both scales and distribution patterns. In addition, to mitigate myopic decisions, we propose a Parameter-Free Cross-Attention (PFCA) that prioritizes the node selected at the preceding time step during decoding. Specifically, PFCA efficiently integrates information about the vehicle selected in the $t - 1$ th time step into the node embeddings. Subsequently, ECHO selects a feasible vehicle-node pair at the t th time step based on the updated node embeddings and current vehicle embeddings (see Section 4.2 for more details). As shown in Fig. 1(b), in the third decoding step, vehicle m_2 is selected to visit the node n_2 instead of vehicle m_3 , ultimately yielding a superior solution. Finally, we propose a tailored data augment method for MMHCVRP, which effectively generates diverse instances by leveraging vehicle permutation invariance and node symmetry to stabilize the RL training process.

To assess the effectiveness of the proposed ECHO, we conduct extensive experiments on MMHCVRP instances with different numbers of vehicles and nodes. The experimental results demonstrate that ECHO outperforms the other NCO solvers designed for MMHCVRP, including two AR-based NCO solvers, namely DRL [22] and 2D-Ptr [23], as well as one PAR-based solver, namely PARCO [25]. Notably, ECHO reduces the average gap by approximately 3% compared to the state-of-the-art (SOTA) solver PARCO across all vehicle and node scales (see Section 5.2). In addition, ECHO exhibits robust cross-scale and cross-distribution generalization ability. Finally, ablation studies demonstrate the effectiveness of the proposed dual-modality node encoder, PFCA mechanism, and data augment method.

The key contributions of this work are as follows:

- We propose a dual-modality node encoder, which effectively exploits the cross attention to fuse node and edge features, thereby capturing local topological relationships.
- We propose a novel decoder that integrates the tailored PFCA mechanism, enabling the solver to focus more on the vehicle selected in the preceding decoding step.
- We propose an efficient data augment method for the MMHCVRP,

which exploits problem-specific symmetries to avoid local minima and stabilize the training process.

- The experimental results demonstrate that the proposed ECHO achieves SOTA performance compared to both AR- and PAR-based NCO solvers, while also demonstrating high-level generalization ability. Moreover, ablation studies validate the effectiveness of all proposed methods.

2. Related Work

In this section, we first introduce general NCO solvers for VRPs, and then discuss the existing efforts for solving the more complex MMHCVRP.

2.1. NCO solvers for VRP

Existing NCO solvers for VRP can be broadly categorized into two types, namely Learning to Construct and Learning to Improve solvers [26–28]. Specifically, inspired by sequence-to-sequence models in the machine translation task, Learning to Construct solvers sequentially select unvisited nodes and append them to partial solutions to construct the complete solutions [29–31]. In contrast, Learning to Improve solvers, motivated by ruin-and-repair heuristics, iteratively perturb and repair current complete solutions to explore (sub-)optimal solutions within a given time frame [32–34]. Among these two paradigms, the Learning-to-Construct solver is more prevalent.

As highlighted in the recent survey by Wu et al. [11], although these solvers have achieved significant progress, they still encounter certain limitations. Specifically, existing NCO solvers exhibit poor cross-scale and cross-distribution generalization abilities and cannot solve large-scale VRPs in real-time [18, 35–37]. In addition, their applicability remains largely confined to TSP and CVRP, with limited success on more complex VRP variants [20, 21]. An important variant is the min-max VRP, where the objective is to minimize the maximum route duration across the entire vehicle fleet. Although several studies have examined the min-max TSP [24, 38–41], they overlook vehicle heterogeneity, and the simplified constraints of min-max TSP hinder applicability to real-world routing scenarios. Consequently, it is essential to investigate the MMHCVRP, which incorporates these additional practical constraints.

2.2. NCO solvers Specifically Designed for MMHCVRP

To better solve the more challenging MMHCVRP, Li et al. [22] introduced DRL, the first AR-based solver tailored for this problem. Specifically, DRL employs an attention-based encoder and a Fully Connected Network (FCN) to embed vehicle and node features, respectively. During decoding, at each time step, it employs a policy network that first selects a vehicle and then chooses that vehicle’s next node to visit, iteratively constructing complete routes until all customer nodes have been visited. Building on the prior study [22], Liu et al. [23] proposed 2D-Ptr, which incorporates a more efficient decoder. Specifically, at each time step, 2D-Ptr directly computes the dot product between vehicle and node embeddings, and selects the vehicle-node pair with the highest scores as the current vehicle and its next node to visit. Compared to DRL’s sequential first-vehicle-then-node selection, 2D-Ptr’s joint selection of vehicle-node pair significantly enhances the computational efficiency. However, both AR-based NCO solvers overlook critical MMHCVRP properties, namely local topological relationships, vehicle permutation invariance, and node symmetry. In addition, they disregard the priority of the previously selected vehicle during the decoding process, resulting in suboptimal solutions.

Unlike AR methods that sequentially select one vehicle and its next node to visit at each time step, Berto et al. [25] proposed PARCO, a PAR-based solver for MMHCVRP that simultaneously selects each vehicle’s next node at every decoding step. Theoretically, PAR-based solvers require only $\frac{1}{M}$ of the time steps of AR-based solvers, where M denotes the number of vehicles, thereby achieving superior efficiency. However, PAR-based solvers suffer from a high-dimensional joint action space that complicates training and necessitates conflict handlers among vehicles, thereby limiting their performance [24].

3. Preliminary

In this section, we first introduce the definition of MMHCVRP, then present the Markov Decision Process (MDP) formula used in our method.

3.1. Definition of MMHCVRP

Consider an MMHCVRP instance $G(\mathbb{M}, \mathbb{N})$, where $\mathbb{M} = \{m_i\}_{i=1}^M$ denotes a fleet of M heterogeneous vehicles, and $\mathbb{N} = \{n_j\}_{j=0}^N$ denotes a set of nodes comprising a depot n_0 and the number of N customers. In this problem,

Table 1: Notations Used in MDP

| Notation | Definition | Category |
|------------------|---|----------|
| χ_i | Speed of i th vehicle | Static |
| ρ_i | Capacity of i th vehicle | Static |
| $\hat{\rho}_i^t$ | Accumulated usage capacity of i th vehicle at t th step | Dynamic |
| δ_i^t | Accumulated travel time of i th vehicle at t th step | Dynamic |
| ℓ_i^t | The last visited node of i th vehicle | Dynamic |
| x_j | X-coordinate of the j th node | Static |
| y_j | Y-coordinate of the j th node | Static |
| d_j^t | Demand of j th node at t th step | Dynamic |

each fully loaded vehicle departs from the depot and visits a sequence of customers to satisfy their demands, subject to the constraints that each customer is visited exactly once and the load carried by any vehicle along its route does not exceed its capacity. Each vehicle m_i is characterized by two attributes, namely, capacity ρ_i and speed χ_i . Each node n_i is described by three attributes, namely, coordinates x_j and y_j , as well as demand q_j . In addition, the objective is to minimize the maximum route duration among all vehicles, which are defined as follows:

$$\min \max_{i \in \mathbb{M}} \left(\sum_{j=1}^{|\gamma_i|} \frac{\text{dist}(\gamma_i^{j-1}, \gamma_i^j)}{\chi_i} + \frac{\text{dist}(\gamma_i^{|\gamma_i|}, \gamma_i^0)}{\chi_i} \right), \quad (1)$$

where γ_i denotes the route of the i th vehicle, and γ_i^j denotes the j th visiting node of the i th vehicle. Functions $|\cdot|$ and $\text{dist}(\cdot, \cdot)$ denote the cardinality operator and distance between two sequential nodes, respectively.

3.2. Markov Decision Process

Following the prior studies [22, 23], we adopt the AR paradigm and define an identical MDP to derive the visitation sequence $\tau = \{(m^t, n^t), t = \{0, 1, \dots, T-1\}\}$ for solving the MMHCVRP. Specifically, the MDP comprises the following five components:

3.2.1. State

The current state is defined as $s^t = (m_i^t, n_i^t), i \in \{1, \dots, M\}, j \in \{0, \dots, N\}$, where m_i^t denotes the i th vehicle's state comprising of $(\chi_i, \rho_i, \hat{\rho}_i^t, \delta_i^t, \ell_i^t)$ and

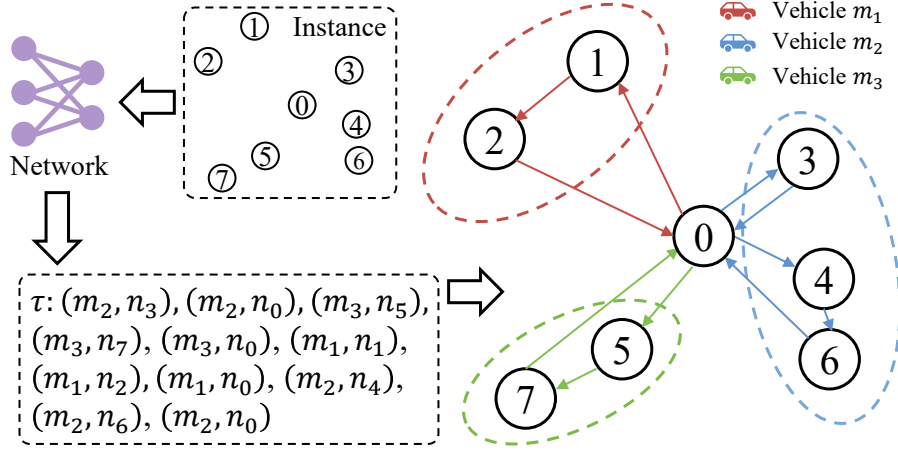


Figure 2: Illustration of solution process for an MMHCVRP instance with three vehicles and eight nodes (seven customer nodes and one depot node). At each time step, the policy network selects a vehicle and a node as the action, repeating until all customer nodes have been served and all vehicles have returned to the depot.

n_i^t denotes the j th node's state comprising of (x_j, y_j, q_j^t) . The definitions of these notations are presented in Table 1.

3.2.2. Action

The action a^t is defined as selecting a vehicle-node pair (m_i^t, n_j^t) , indicating that the i th vehicle is selected to visit the j th node at the t th time step. Note that, the action space comprises only valid vehicle-node combinations, while invalid pairs are masked, e.g., those involving customer nodes that have already been visited.

3.2.3. Transaction

Given the current state s^t and action $a^t = (m_i^t, n_j^t)$, the next state $s^{t+1} = f(s^t, a^t)$ is obtained by updating each vehicle's accumulated usage capacity, accumulated travel time, and current location, as well as each node's demand. For every vehicle $k \in \{1, \dots, M\}$ and node $l \in \{0, \dots, N\}$, these updates are defined as follows:

$$\hat{\rho}_k^{t+1} = \begin{cases} 0, & k = i, j = 0, \\ \hat{\rho}_k^t + d_j, & k = i, j \neq 0, \\ \hat{\rho}_k^t, & \text{otherwise.} \end{cases} \quad (2)$$

$$\delta_k^{t+1} = \begin{cases} \delta_k^t + \frac{dist(n_j, \ell_i^t)}{\chi_m}, & k = i, \\ \delta_k^t, & \text{otherwise.} \end{cases} \quad (3)$$

$$\ell_k^{t+1} = \begin{cases} n_j, & k = i, \\ \ell_k^t, & \text{otherwise.} \end{cases} \quad (4)$$

$$d_l^{t+1} = \begin{cases} 0, & l = j, \\ d_l^t, & \text{otherwise.} \end{cases} \quad (5)$$

3.2.4. *Reward*

The total reward R is defined as the negative of the longest travel time across all vehicles, as follows:

$$R = - \max_{i \in \{1, \dots, M\}} \delta_i^T, \quad (6)$$

where δ_i^T denotes the accumulated travel time of the i th vehicle at final step, and M denotes the number of vehicles.

3.2.5. *Policy*

Given the current state s_t , the policy selects an action according to the probability produced by the neural network. This process continues until all customer nodes are visited and all vehicles return to the depot, concluding the episode and resulting in the construction of a valid tour. In Fig. 2, we illustrate the visiting sequence generated by the policy network for an MMHCVRP instance.

4. ECHO

The illustration of ECHO is schematically presented in Fig. 3. In this section, we first introduce the customized dual-modality node encoder and the adopted vehicle encoder for MMHCVRP, then detail the PFCA mechanism-based decoder, and finally present the proposed data augment method along with the corresponding RL training algorithm.

4.1.1. Node Encoder

To capture the local topological relationships among nodes while mitigating interference from irrelevant nodes, we propose a dual-modality node encoder, which integrates edge attributes (i.e., topological distances) with node attributes (i.e., coordinates and demands). Specifically, ECHO first exploits two FCNs to embed the initial node and edge features, respectively. Let $u_j = (x_j, y_j, d_j^t)$ denote the initial attributes of the j th node, and let e_j be the vector of distances from the j th node to all other nodes. The node and edge features are then computed as follows:

$$U_j = \begin{cases} u_j \mathbf{W}_{no} + \text{DT}, & j = 0, \\ u_j \mathbf{W}_{no}, & \text{otherwise.} \end{cases} \quad (7)$$

$$E_j = e_j \mathbf{W}_{ed}, \quad (8)$$

where $j \in \{0, \dots, N\}$, and the trainable parameters include $\mathbf{W}_{no} \in \mathbb{R}^{3 \times d}$, $\mathbf{W}_{ed} \in \mathbb{R}^{N \times d}$ and the depot token $\text{DT} \in \mathbb{R}^d$. Following the prior study [23], we exploit a learnable depot token to distinguish the depot from customer nodes during training.

Then, the node encoder exploits the number of L stacked Multi-Head Self-Attention Blocks to facilitate information exchange among node attributes. Let $H^0 = \{U_0, \dots, U_N\}$, the node embedding H^{l+1} is computed as follows:

$$\bar{H}^l = \text{BN} (H^l + \text{MHA}_{\text{self}} (H^l, H^l, H^l)), \quad (9)$$

$$H^{l+1} = \text{BN} (\bar{H}^l + \text{FF} (\bar{H}^l)), \quad (10)$$

where BN denotes the batch normalization. The functions FF and MHA_{self} denote a two-layer feed-forward network with ReLU activation function and the multi-head self-attention mechanism, respectively. They are defined as follows:

$$\text{FF}(\bar{H}^l) = \left(\text{ReLU}(\bar{H}^l \mathbf{W}_1) \right) \mathbf{W}_2, \quad (11)$$

$$\text{MHA}_{\text{self}}(Q, K, V) = (\|_{k=1}^8 \text{ATT}_k(Q, K, V)) \mathbf{W}^O, \quad (12)$$

$$\text{ATT}_k(Q, K, V) = \text{softmax} \left(\frac{(Q \mathbf{W}_{Q,k})(K \mathbf{W}_{K,k})^T}{\sqrt{d'}} \right) V \mathbf{W}_{V,k}, \quad (13)$$

where $\mathbf{W}_1 \in \mathbb{R}^{d \times 4d}$, $\mathbf{W}_2 \in \mathbb{R}^{4d \times d}$, $\mathbf{W}^O \in \mathbb{R}^{d \times d}$ and $\mathbf{W}_Q, \mathbf{W}_K, \mathbf{W}_V \in \mathbb{R}^{d \times d'}$ are trainable parameters, and the number of head is set to 8, i.e., $d' = d/8$. The symbol $\|$ denotes the concatenation operator.

Subsequently, the node encoder exploits the vanilla cross-attention mechanism to integrate the extracted local topological features E with the node embedding H^L produced by the multi-head self-attention blocks.

$$\mathbf{N} = H^L + \alpha \text{MHA}_{\text{cross}}(H^L, E, E), \quad (14)$$

where $\text{MHA}_{\text{cross}}$ is computed analogously to MHA_{self} in Eq. (12), except that the query Q is derived from H^L while the key K and value V are derived from E . The symbol α denotes the gating coefficient, defined as follows:

$$\alpha = \text{Sigmoid}\left(\left(\text{MHA}_{\text{cross}}(H^L, E, E) \parallel H^L\right) \mathbf{W}_g\right), \quad (15)$$

where $\mathbf{W}_g \in \mathbb{R}^{2d \times 1}$. By adopting this design, ECHO efficiently integrates local topological features into the node embedding. It is worth mentioning that while certain studies [42, 43] also highlight the importance of local topological relationships, ECHO departs fundamentally in its methodology. Specifically, our ECHO learns to aggregate the local topological features in the embedding space, whereas these prior studies reshape attention scores among nodes during decoding using these features.

4.1.2. Vehicle Encoder

Because each vehicle’s current location corresponds to a node’s coordinates, the vehicle embedding should inherently incorporate the associated node embedding. Therefore, the vehicle encoder must fuse these node embeddings with vehicle-specific attributes to produce the vehicle embedding. To this end, we adopt the vehicle encoder architecture proposed by the prior study [23]. Specifically, similar to the node encoder, the vehicle encoder first embeds the vehicle attributes (i.e., $\chi_i, \rho_i, \hat{\rho}_i^t$, and δ_i^t , see Table 1 for definitions about these attributes), using two fully connected layers with ReLU activations, as follows:

$$\mathbf{M}_i^{1,t} = \left[\text{ReLU}\left(\left(\chi_i, \rho_i, \hat{\rho}_i^t, \delta_i^t\right) \mathbf{W}_3\right) \right] \mathbf{W}_4 + \text{PE}_i^t \mathbf{W}_{pe} \quad (16)$$

where $\mathbf{W}_3 \in \mathbb{R}^{d \times 4d}$, $\mathbf{W}_4 \in \mathbb{R}^{4d \times d}$, and $\mathbf{W}_{pe} \in \mathbb{R}^{d \times d}$ are trainable parameters. PE_i^t denotes the embedding of the node most recently visited by the i th vehicle at the t th time step. It is worth mentioning that, unlike the node encoder, the vehicle encoder needs to update vehicle embeddings throughout the decoding process to reflect changes in vehicle attributes.

Subsequently, the vehicle encoder applies a self-attention layer to facilitate inter-vehicle communication, followed by a vanilla cross-attention layer to infuse each vehicle embedding with contextual information from node embeddings. The vehicle embedding \mathbf{M}^t is computed as follows:

$$\mathbf{M}^{2,t} = \mathbf{M}^{1,t} + \text{MHA}_{\text{self}}(\mathbf{M}^{1,t}, \mathbf{M}^{1,t}, \mathbf{M}^{1,t}), \quad (17)$$

$$\mathbf{M}^t = \mathbf{M}^{2,t} + \text{MHA}_{\text{cross}}(\mathbf{M}^{2,t}, \mathbf{N}^{\text{mask}}, \mathbf{N}^{\text{mask}}), \quad (18)$$

where MHA_{self} and $\text{MHA}_{\text{cross}}$ denote the self-attention and cross-attention operations, respectively, \mathbf{N}^{mask} denotes the node embedding with all visited nodes masked out. Finally, the vehicle embedding \mathbf{M}^t and \mathbf{N} are fed into the decoder to effectively select the vehicle-node pair at each time step.

4.2. Decoder of ECHO

To efficiently select vehicle-node pairs, we design a decoder inspired by the CLIP architecture [44]. While the prior study [23] also employed a similar CLIP-based architecture, our decoder incorporates fundamentally different structural components. In particular, we propose a **Parameter-Free Cross Attention (PFCA)** mechanism, which explicitly amplifies the influence of the node selected at the $t - 1$ th time step, thereby reducing myopic decision-making.

Specifically, given the vehicle embedding $\mathbf{M}^t \in \mathbb{R}^{M \times d}$ and node embedding $\mathbf{N} \in \mathbb{R}^{(N+1) \times d}$ produced by their respective encoders, the proposed decoder first integrates the vehicle embedding selected at the $t - 1$ th time step, \mathbf{M}_s^{t-1} , with the node embedding \mathbf{N} to yield the updated node embedding $\hat{\mathbf{N}}^t$, computed as follows:

$$\hat{\mathbf{N}}^t = \begin{cases} \mathbf{N}, & t = 0, \\ \text{PFCA}(\mathbf{M}_s^{t-1}, \mathbf{N}), & \text{otherwise,} \end{cases} \quad (19)$$

$$\text{PFCA}(\mathbf{M}_s^{t-1}, \mathbf{N}) = \text{softmax}\left(\frac{\mathbf{N}(\mathbf{M}_s^{t-1})^\top}{\sqrt{d}}\right)\mathbf{M}_s^{t-1} + \mathbf{N}. \quad (20)$$

By applying the proposed PFCA mechanism, information from the previously selected vehicle is seamlessly integrated into the node embedding.

Subsequently, the vehicle embedding \mathbf{M}^t and the updated node embedding $\hat{\mathbf{N}}^t$ are combined to compute the attention scores for all vehicle-node pairs at the current time step. In addition, to ensure feasibility, we mask invalid pairs by setting them to $-\infty$. For example, if a vehicle lacks sufficient

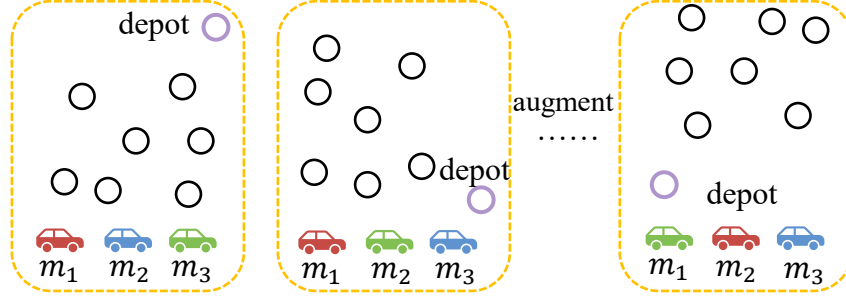


Figure 4: Illustration of the proposed augment method.

remaining capacity to fulfill a node’s demand, its corresponding vehicle-node pair is masked. Formally, the attention score $\beta_{i,j}^t$ is defined as follows:

$$\beta_{i,j}^t = \begin{cases} -\infty, & d_j^t = 0 \wedge j \neq 0, \\ -\infty, & \ell_i^t = 0 \wedge j = 0, \\ -\infty, & \rho_i - \hat{\rho}_i^t < d_j^t, \\ \lambda \tanh\left(\frac{\mathbf{M}_i^t \hat{\mathbf{N}}_j^t}{\sqrt{d}}\right), & \text{otherwise,} \end{cases} \quad (21)$$

where $\tanh(\cdot)$ denotes the hyperbolic tangent activation function, λ denotes the hyper-parameter set identically to that in the prior study [23].

Finally, the probability of selecting vehicle-node pair (m_i, n_j) at the t th time step is defined as follows:

$$p_{i,j}^t = \text{softmax}(\beta_{i,j}^t). \quad (22)$$

After computing the probability distribution, ECHO constructs solutions for the given MMHCVRP instance using either Greedy or Sampling strategies (see Section 5.1 for more details on these strategies).

4.3. Data Augment Method

Data augment techniques have been widely applied to stabilize the RL-based training process of NCO solvers in canonical single-vehicle VRPs [45, 46]. However, in the single-vehicle setting, these methods need only exploit the node symmetry of the VRP. In contrast, MMHCVRP exhibits both node symmetry and vehicle-permutation invariance. To the best of our knowledge,

Table 2: Node Augment Transformations

| $f(x, y)$ | |
|------------------|------------------|
| (x, y) | (y, x) |
| $(x, 1 - y)$ | $(y, 1 - x)$ |
| $(1 - x, y)$ | $(1 - y, x)$ |
| $(1 - x, 1 - y)$ | $(1 - y, 1 - x)$ |

no prior work has simultaneously considered both intrinsic properties in solving the MMHCVRP, which may underlie their suboptimal performance.

As shown in Fig. 4, to address this open challenge, we propose a tailored data augment method that integrates vehicle permutation invariance and node symmetry. Specifically, following the node augment approach of prior study [45], we generate $K = 8$ augmentations per instance by reflecting node coordinates across multiple axes, as shown in Table 2. Concurrently, for each augmented instance, we sample a random vehicle permutation of the vehicle set. Note that, since the total number of vehicle permutations $M!$ may be smaller than K , duplicate permutations across augmentations are unavoidable (e.g., for $M = 3$, $3! = 6 < 8$).

We train ECHO using the well-known REINFORCE algorithm [47] with a shared baseline similar to the prior studies [45, 46]. As detailed in Section 3.1, the objective of MMHCVRP is to minimize the maximum vehicle travel time. Accordingly, we define the total reward R as the negative of this objective. The policy gradient is computed as follows:

$$\nabla_{\theta} \mathcal{L} = \frac{1}{B \cdot K} \sum_{i=1}^B \sum_{j=1}^K \left(R(\tau_{i,j} | S_i) - b(S_i) \right) \cdot \nabla_{\theta} \log p_{\theta}(\tau_{i,j} | S_i), \quad (23)$$

where B and K denote the batch size and the number of augmentations per instance, respectively, and $b(\cdot)$ denotes the shared baseline, computed as the average reward across all augmentations.

5. Experimental Results

To assess the performance of ECHO, we conduct extensive experiments in this section. Section 5.1 first describes datasets, baseline methods, and

Table 3: Performance Comparison of different Algorithms on HCVRP Instances across Varying Node Scales $N = 60, 100$ with a Fixed Vehicle Number $M = 3$

| M | 3 | | | | | |
|------------------------------------|-------------|-------------|------------|--------------|-------------|------------|
| N | 60 | | | 100 | | |
| Metric | Obj. ↓ | Gap (%) ↓ | Time (s) ↓ | Obj. ↓ | Gap (%) ↓ | Time (s) ↓ |
| SISR † | 6.57 | - | 271 | 10.29 | - | 615 |
| GA † | 9.21 | 40.18 | 233 | 15.33 | 48.98 | 479 |
| SA † | 7.04 | 7.15 | 130 | 11.13 | 8.16 | 434 |
| AM (ICLR'19) † (<i>g.</i>) | 8.49 | 29.22 | 0.08 | 12.68 | 23.23 | 0.14 |
| ET (AAAI'24) † (<i>g.</i>) | 7.58 | 15.37 | 0.15 | 11.74 | 14.09 | 0.25 |
| DPN (ICML'24) † (<i>g.</i>) | 7.50 | 14.16 | 0.18 | 11.54 | 12.15 | 0.30 |
| DRL (TCYB'22) † (<i>g.</i>) | 7.43 | 13.09 | 0.19 | 11.44 | 11.18 | 0.32 |
| 2D-Ptr (AAMAS'24) (<i>g.</i>) | 7.20 | 9.59 | 0.04 | 11.12 | 8.07 | 0.08 |
| PARCO (NeurIPS'25) † (<i>g.</i>) | 7.12 | 8.37 | 0.04 | 10.98 | 6.71 | 0.06 |
| ECHO (ours) (<i>g.</i>) | 6.83 | 3.93 | 0.05 | 10.68 | 3.82 | 0.07 |
| AM (ICLR'19) † (<i>s.</i>) | 7.62 | 15.98 | 0.14 | 11.82 | 14.87 | 0.29 |
| ET (AAAI'24) † (<i>s.</i>) | 7.14 | 8.68 | 0.21 | 11.20 | 8.84 | 0.41 |
| DPN (ICML'24) † (<i>s.</i>) | 7.08 | 7.76 | 0.25 | 11.04 | 7.29 | 0.48 |
| DRL (TCYB'22) † (<i>s.</i>) | 6.97 | 6.09 | 0.30 | 10.90 | 5.93 | 0.60 |
| 2D-Ptr (AAMAS'24) (<i>s.</i>) | 6.82 | 3.81 | 0.07 | 10.71 | 4.08 | 0.13 |
| PARCO (NeurIPS'25) † (<i>s.</i>) | 6.82 | 3.81 | 0.05 | 10.61 | 3.11 | 0.08 |
| ECHO (ours) (<i>s.</i>) | 6.64 | 1.01 | 0.28 | 10.44 | 1.50 | 0.49 |

evaluation metrics. Section 5.2 then compares the performance of different NCO solvers. Next, Section 5.3 evaluates the generalization ability of ECHO across different scales and distribution patterns. Finally, Section 5.4 conducts ablation studies to assess the effectiveness of all proposed components.

5.1. Experimental Settings

Datasets and Hardware configuration: Following the prior studies [22, 23], we assess the performance of ECHO on MMHCVRP instances with varying numbers of vehicles and nodes. Except for the cross-distribution generalization experiments in Section 5.3, the coordinates of customer nodes and depot node are uniformly sampled from the unit square $[0, 1] \times [0, 1]$, and the demand of customer nodes are uniformly sampled from the set $\{1, 2, \dots, 9\}$. For vehicles, capacities are uniformly sampled from $\{20, 21, \dots, 40\}$, and speeds are uniformly sampled from the interval $[0.5, 1]$. For each vehicle and node scale, the training dataset comprises the number of 1,280,000 instances, and the test dataset comprises 10,000 instances. All experiments are conducted on a computer equipped with an Intel(R) Core(TM) i9-12900K CPU

Table 4: Performance Comparison of different Algorithms on HCVRP Instances across Varying Node Scales $N = 60, 100$ with a Fixed Vehicle Number $M = 5$

| M | 5 | | | | | |
|------------------------------------|-------------|-------------|------------|-------------|-------------|------------|
| N | 60 | | | 100 | | |
| Metric | Obj. ↓ | Gap (%) ↓ | Time (s) ↓ | Obj. ↓ | Gap (%) ↓ | Time (s) ↓ |
| SISR † | 4.00 | - | 274 | 6.17 | - | 623 |
| GA † | 6.89 | 72.25 | 320 | 10.93 | 77.15 | 623 |
| SA † | 4.39 | 9.75 | 289 | 6.80 | 10.21 | 557 |
| AM (ICLR'19) † (<i>g.</i>) | 5.51 | 37.75 | 0.08 | 8.10 | 31.28 | 0.13 |
| ET (AAAI'24) † (<i>g.</i>) | 4.76 | 19.00 | 0.17 | 7.25 | 17.50 | 0.25 |
| DPN (ICML'24) † (<i>g.</i>) | 4.60 | 15.00 | 0.19 | 6.94 | 12.48 | 0.40 |
| DRL (TCYB'22) † (<i>g.</i>) | 4.71 | 17.75 | 0.22 | 7.06 | 14.42 | 0.37 |
| 2D-Ptr (AAMAS'24) (<i>g.</i>) | 4.48 | 12.00 | 0.05 | 6.75 | 9.40 | 0.08 |
| PARCO (NeurIPS'25) † (<i>g.</i>) | 4.40 | 10.00 | 0.05 | 6.61 | 7.13 | 0.05 |
| ECHO (ours) (<i>g.</i>) | 4.18 | 4.60 | 0.06 | 6.40 | 3.74 | 0.09 |
| AM (ICLR'19) † (<i>s.</i>) | 4.82 | 20.50 | 0.13 | 7.45 | 20.75 | 0.28 |
| ET (AAAI'24) † (<i>s.</i>) | 4.46 | 11.50 | 0.22 | 6.85 | 11.02 | 0.38 |
| DPN (ICML'24) † (<i>s.</i>) | 4.35 | 8.75 | 0.28 | 6.66 | 7.94 | 0.52 |
| DRL (TCYB'22) † (<i>s.</i>) | 4.34 | 8.50 | 0.36 | 6.65 | 7.78 | 0.76 |
| 2D-Ptr (AAMAS'24) (<i>s.</i>) | 4.20 | 5.00 | 0.08 | 6.46 | 4.70 | 0.16 |
| PARCO (NeurIPS'25) † (<i>s.</i>) | 4.17 | 4.25 | 0.05 | 6.36 | 3.08 | 0.08 |
| ECHO (ours) (<i>s.</i>) | 4.03 | 0.96 | 0.37 | 6.24 | 1.12 | 0.51 |

and an NVIDIA RTX 4090 GPU (24GB).

Baselines and Evaluation Metrics: We compare ECHO against six NCO benchmarks, including AM [30], DRL [22], ET [41], DPN [24], 2D-Ptr [23], and PARCO [25]. Of these, DRL, 2D-Ptr, and PARCO are specifically designed for the MMHCVRP, ET and DPN target the Min-max TSP, and AM is tailored to TSP and CVRP. In addition, following the prior studies [22, 23], we also include the heuristic algorithms GA [48], SA [49], and the SOTA SISR [50] for comparison. The evaluation metrics include the objective value (Obj.), Gap, and computation time (Time), where Gap is defined as the relative difference in the "objective value" between each method and the SISR heuristic. In addition, for NCO solvers, we report the results under two decoding strategies, namely Greedy and Sampling decoding strategies. With Greedy decoding, the solver always selects vehicle(s) and node(s) with the maximum probability at each time step. Whereas the sampling strategy randomly selects vehicle(s) and node(s) utilizing the learned probability, constructs the number of k candidate solutions, and ultimately reports the best among them. In all experiments conducted in the paper, k is set to 1280,

Table 5: Performance Comparison of different Algorithms on HCVRP Instances across Varying Node Scales $N = 60, 100$ with a Fixed Vehicle Number $M = 7$

| M | 7 | | | | | |
|------------------------------------|-------------|-------------|------------|-------------|-------------|------------|
| N | 60 | | | 100 | | |
| Metric | Obj. ↓ | Gap (%) ↓ | Time (s) ↓ | Obj. ↓ | Gap (%) ↓ | Time (s) ↓ |
| SISR † | 2.91 | - | 276 | 4.45 | - | 625 |
| GA † | 5.98 | 105.50 | 405 | 9.10 | 104.49 | 772 |
| SA † | 3.30 | 13.40 | 362 | 5.01 | 12.58 | 678 |
| AM (ICLR'19) † (<i>g.</i>) | 4.15 | 42.61 | 0.09 | 6.13 | 37.75 | 0.13 |
| ET (AAAI'24) † (<i>g.</i>) | 3.58 | 23.02 | 0.16 | 5.23 | 17.53 | 0.26 |
| DPN (ICML'24) † (<i>g.</i>) | 3.45 | 18.56 | 0.26 | 4.98 | 11.91 | 0.43 |
| DRL (TCYB'22) † (<i>g.</i>) | 3.60 | 23.71 | 0.25 | 5.38 | 20.90 | 0.43 |
| 2D-Ptr (AAMAS'24) (<i>g.</i>) | 3.31 | 13.75 | 0.05 | 4.92 | 10.56 | 0.08 |
| PARCO (NeurIPS'25) † (<i>g.</i>) | 3.25 | 11.68 | 0.05 | 4.79 | 7.64 | 0.05 |
| ECHO (ours) (<i>g.</i>) | 3.05 | 4.71 | 0.06 | 4.61 | 3.61 | 0.09 |
| AM (ICLR'19) † (<i>s.</i>) | 3.63 | 24.74 | 0.14 | 5.58 | 25.39 | 0.28 |
| ET (AAAI'24) † (<i>s.</i>) | 3.33 | 14.43 | 0.22 | 4.98 | 11.91 | 0.40 |
| DPN (ICML'24) † (<i>s.</i>) | 3.20 | 9.97 | 0.38 | 4.79 | 7.64 | 0.78 |
| DRL (TCYB'22) † (<i>s.</i>) | 3.25 | 11.68 | 0.43 | 4.98 | 11.91 | 0.92 |
| 2D-Ptr (AAMAS'24) (<i>s.</i>) | 3.09 | 6.19 | 0.09 | 4.68 | 5.17 | 0.18 |
| PARCO (NeurIPS'25) † (<i>s.</i>) | 3.06 | 5.15 | 0.07 | 4.58 | 2.92 | 0.09 |
| ECHO (ours) (<i>s.</i>) | 2.93 | 0.98 | 0.47 | 4.48 | 0.77 | 1.14 |

following the precedent established by [30].

5.2. Performance Comparison

In Tables 3~5, we compare the performance of ECHO against various heuristics and NCO solvers on MMHCVRP instances with varying numbers of vehicles ($M = 3, 5, 7$) and nodes ($N = 60, 100$). As shown in Tables 3~5, ECHO achieves SOTA performance across varying numbers of vehicles and nodes compared with the other NCO solvers. When adopting the sampling decoding strategy, ECHO reduces the average gap to 3.77% and 2.67% relative to the AR-based 2D-Ptr and PAR-based PARCO solvers, respectively. The high-level performance reflects the combined contributions of all proposed components and methods (see Section 5.4). Notably, even under greedy decoding, ECHO matches PARCO's performance in gap achieved with sampling. Compared to the SOTA heuristic SISR, ECHO exhibits an average gap of approximately 1%, while running over 100× faster, making it more suitable for time-sensitive real-world scenarios.

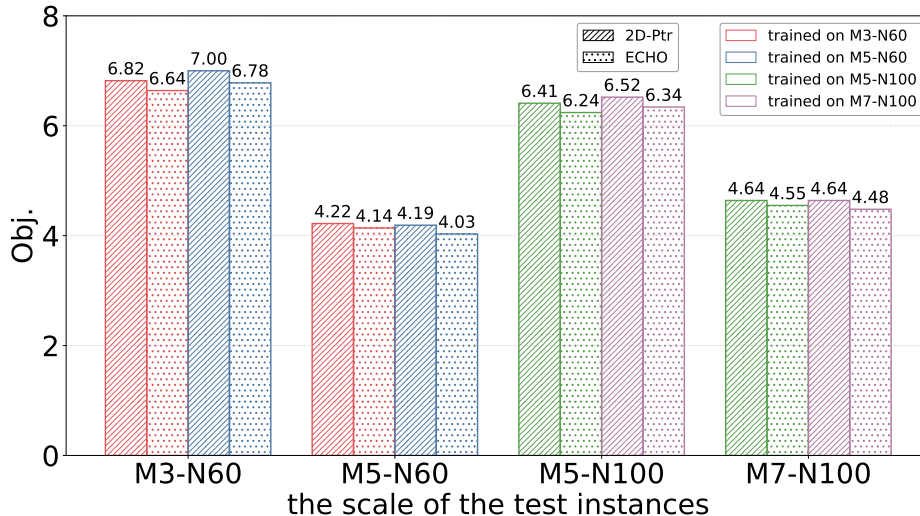


Figure 5: Generalization performance of NCO solvers across different vehicle scales.

5.3. Generalization Studies

To assess the cross-scale and cross-distribution generalization abilities of ECHO, we conduct extensive experiments in this subsection. Specifically, in Figs. 5 and 6, we present the generalization performance of ECHO versus 2D-Ptr across varying node and vehicle scales, respectively. The abbreviation M3-N60 denotes a configuration with three vehicles and 60 nodes. In Fig. 7, we assess the cross-distribution generalization performance of ECHO and 2D-Ptr. To generate clustered test instances, following the procedure of the prior study [51], we sample three cluster centers for each instance, assign each node uniformly to one center, and perturb each node’s coordinates with Gaussian noise to induce the clustered distribution.

As shown in Fig. 5, ECHO achieves comparable cross-vehicle scale generalization performance to 2D-Ptr. Furthermore, even when trained exclusively on non-target vehicle scales, ECHO still outperforms 2D-Ptr trained directly on the target scale. For example, when trained on the M5-N60 configuration, ECHO attains an objective value of 6.78 on M3-N60, compared to 6.82 achieved by 2D-Ptr trained and evaluated on M3-N60. As shown in Fig. 6, ECHO also achieves high-level cross-node scale generalization ability compared to 2D-Ptr. As shown in Fig. 7, under the clustered distribution, ECHO consistently outperforms 2D-Ptr across all vehicle and node scales. This advantage arises from our dual-modality encoder, which more effec-

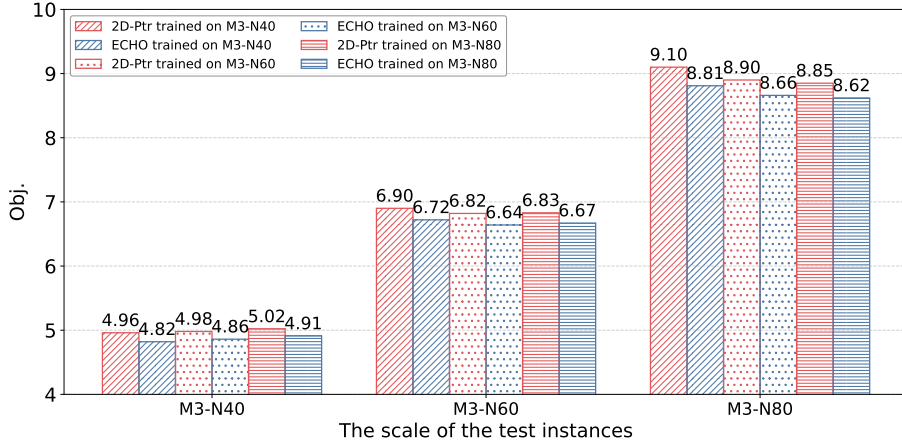


Figure 6: Generalization performance of NCO solvers across different node scales.

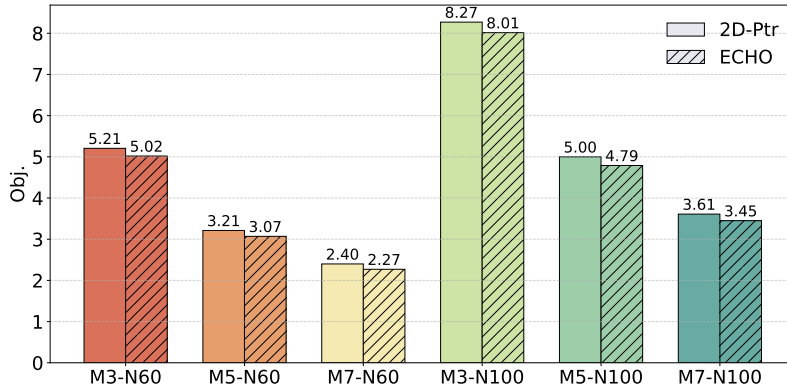


Figure 7: Generalization performance of NCO solvers across different distribution patterns.

tively captures local topological relationships among nodes, thereby reducing sensitivity to distribution shifts.

5.4. Ablation Studies

In this subsection, we conduct ablation studies to investigate the contributions of key ECHO design components. The performance is evaluated on MMHCVRP instances with the number of three vehicles and 60 nodes, and the results are presented in Table 6. Specifically, in w/o dual-modality encoder, the node encoder processes only node attributes, ignores edge attributes, and disables the cross-attention operator used to fuse edge and node

Table 6: Ablation Study Results on Different Design Choices

| Algorithm | Gap (%) |
|---------------------------|---------|
| w/o dual-modality encoder | 1.82 |
| w/o PFCA mechanism | 1.28 |
| w/o vehicle augment | 1.20 |
| ECHO | 1.01 |

features. In w/o PFCA mechanism, the decoder omits historical vehicle information by disabling the PFCA mechanism. In w/o vehicle augment, only node data are augmented following the prior study [45], while vehicle data remain unchanged. As shown in Table 6, the experimental results demonstrate that each component contributes to the SOTA performance of ECHO.

6. Conclusion

To better address the practical challenges of MMHCVRP, we propose ECHO, a novel NCO solver. Specifically, ECHO employs our proprietary dual-modality node encoder to capture local topological relationships among nodes. In addition, by incorporating the proposed PFCA mechanism, ECHO mitigates myopic decisions by emphasizing vehicles selected in the preceding decoding step. Finally, to stabilize the RL training process, ECHO introduces the tailored data augment method that leverages MMHCVRP’s inherent properties, i.e., vehicle permutation invariance and node symmetry. The experimental results demonstrate the effectiveness of ECHO across varying numbers of vehicles and nodes, its robust generalization across scales and distribution patterns, and the contribution of each designed methods.

7. Acknowledgments

This work is supported in part by the Jilin Provincial Department of Science and Technology Project under Grant 20240101369JC.

References

- [1] Y. Wu, J. Zhou, Y. Xia, X. Zhang, Z. Cao, J. Zhang, Neural airport ground handling, *IEEE Transactions on Intelligent Transportation Systems* 24 (12) (2023) 15652–15666.

- [2] Y. Bengio, A. Lodi, A. Prouvost, Machine learning for combinatorial optimization: A methodological tour d’horizon, *European Journal of Operational Research* 290 (2) (2021) 405–421.
- [3] Y. Xiao, D. Wang, B. Li, H. Chen, W. Pang, X. Wu, H. Li, D. Xu, Y. Liang, Y. Zhou, Reinforcement learning-based non-autoregressive solver for traveling salesman problems, *IEEE Transactions on Neural Networks and Learning Systems* 36 (7) (2025) 13402–13416.
- [4] X. Wu, D. Wang, Z. Cao, C. Wu, L. Wen, C. Miao, Y. Xiao, Y. Zhou, Efficient heuristics generation for solving combinatorial optimization problems using large language models, in: *Proceedings of ACM SIGKDD Conference on Knowledge Discovery and Data Mining, 2025*, pp. 3228–3239.
- [5] W. Yang, D. Wang, W. Pang, A.-H. Tan, Y. Zhou, Goods consumed during transit in split delivery vehicle routing problems: Modeling and solution, *IEEE Access* 8 (2020) 110336–110350.
- [6] K. Li, T. Zhang, R. Wang, W. Qin, H. He, H. Huang, Research reviews of combinatorial optimization methods based on deep reinforcement learning, *Acta Automatica Sinica* 47 (11) (2021) 2521–2537.
- [7] X. Wu, J. Han, D. Wang, P. Gao, Q. Cui, L. Chen, Y. Liang, H. Huang, H. P. Lee, C. Miao, Y. Zhou, C. Wu, Incorporating surprisingly popular algorithm and euclidean distance-based adaptive topology into PSO, *Swarm and Evolutionary Computation* 76 (2023) 101222.
- [8] Z. Lyu, M. Z. Islam, A. J. Yu, A scalable and adaptable supervised learning approach for solving the traveling salesman problems, *IEEE Transactions on Intelligent Transportation Systems* 25 (11) (2024) 17092–17104.
- [9] W. Song, X. Wu, B. Yang, Y. Zhou, Y. Xiao, Y. Liang, H. Ge, H. P. Lee, C. Wu, Towards efficient few-shot graph neural architecture search via partitioning gradient contribution, in: *Proceedings of the ACM SIGKDD Conference on Knowledge Discovery and Data Mining V.2, 2025*, p. 2609–2620.
- [10] X. Wu, D. Wang, H. Chen, L. Yan, Y. Xiao, C. Miao, H. Ge, D. Xu, Y. Liang, K. Wang, C. Wu, Y. Zhou, Neural architecture search for text

- classification with limited computing resources using efficient Cartesian genetic programming, *IEEE Transactions on Evolutionary Computation* 28 (3) (2024) 638–652.
- [11] X. Wu, D. Wang, L. Wen, Y. Xiao, C. Wu, Y. Wu, C. Yu, D. L. Maskell, Y. Zhou, Neural combinatorial optimization algorithms for solving vehicle routing problems: A comprehensive survey with perspectives, arXiv: 2406.00415 (2024).
 - [12] Y. Xiao, D. Wang, X. Wu, Y. Wu, B. Li, W. Du, L. Wang, Y. Zhou, Improving generalization of neural vehicle routing problem solvers through the lens of model architecture, *Neural Networks* 187 (2025) 107380.
 - [13] J. J. Q. Yu, W. Yu, J. Gu, Online vehicle routing with neural combinatorial optimization and deep reinforcement learning, *IEEE Transactions on Intelligent Transportation Systems* 20 (10) (2019) 3806–3817.
 - [14] R. Zhang, C. Zhang, Z. Cao, W. Song, P. S. Tan, J. Zhang, B. Wen, J. Dauwels, Learning to solve multiple-tsp with time window and rejections via deep reinforcement learning, *IEEE Transactions on Intelligent Transportation Systems* 24 (1) (2023) 1325–1336.
 - [15] R. Tian, Z. Sun, L. Chang, J. Wu, X. Lu, Rapid solution for flexible pickup and delivery services problem based on improved actor-critic deep reinforcement learning, *IEEE Transactions on Intelligent Transportation Systems* 26 (6) (2025) 7640–7654.
 - [16] Y. Xiao, D. Wang, B. Li, M. Wang, X. Wu, C. Zhou, Y. Zhou, Distilling autoregressive models to obtain high-performance non-autoregressive solvers for vehicle routing problems with faster inference speed, in: *Proceedings of the AAAI Conference on Artificial Intelligence*, 2024, pp. 20274–20283.
 - [17] L. Xin, W. Song, Z. Cao, J. Zhang, Multi-decoder attention model with embedding glimpse for solving vehicle routing problems, in: *Proceedings of the AAAI Conference on Artificial Intelligence*, 2021, pp. 12042–12049.
 - [18] H. Ye, J. Wang, H. Liang, Z. Cao, Y. Li, F. Li, GLOP: Learning global partition and local construction for solving large-scale routing problems

- in real-time, in: Proceedings of the AAAI Conference on Artificial Intelligence, 2024, pp. 20284–20292.
- [19] M. Wang, Y. Zhou, Z. Cao, Y. Xiao, X. Wu, W. Pang, Y. Jiang, H. Yang, P. Zhao, Y. Li, An efficient diffusion-based non-autoregressive solver for traveling salesman problem, in: Proceedings of the ACM SIGKDD Conference on Knowledge Discovery and Data Mining, 2025, pp. 1469–1480.
- [20] J. Zhou, Z. Cao, Y. Wu, W. Song, Y. Ma, J. Zhang, X. Chi, MVMoE: Multi-task vehicle routing solver with mixture-of-experts, in: Proceedings of the International Conference on Machine Learning, 2024, pp. 61804–61824.
- [21] H. Li, F. Liu, Z. Zheng, Y. Zhang, Z. Wang, CaDA: Cross-problem routing solver with constraint-aware dual-attention, in: Proceedings of the International Conference on Machine Learning, 2025, pp. 35438–35456.
- [22] J. Li, Y. Ma, R. Gao, Z. Cao, A. Lim, W. Song, J. Zhang, Deep reinforcement learning for solving the heterogeneous capacitated vehicle routing problem, *IEEE Transactions on Cybernetics* 52 (12) (2022) 13572–13585.
- [23] Q. Liu, C. Liu, S. Niu, C. Long, J. Zhang, M. Xu, 2d-ptr: 2d array pointer network for solving the heterogeneous capacitated vehicle routing problem, in: Proceedings of the International Conference on Autonomous Agents and Multiagent Systems, 2024, p. 1238–1246.
- [24] Z. Zheng, S. Yao, Z. Wang, T. Xialiang, M. Yuan, K. Tang, DPN: Decoupling partition and navigation for neural solvers of min-max vehicle routing problems, in: Proceedings of the International Conference on Machine Learning, 2024, pp. 61559–61592.
- [25] F. Berto, C. Hua, L. Luttmann, J. Son, J. Park, K. Ahn, C. Kwon, L. Xie, J. Park, Parallel autoregressive models for multi-agent combinatorial optimization, in: Proceedings of Advances in Neural Information Processing Systems, 2025.
- [26] K. Li, F. Liu, Z. Wang, Q. Zhang, Destroy and repair using hypergraphs for routing, in: Proceedings of the AAAI Conference on Artificial Intelligence, 2025, pp. 18341–18349.

- [27] Y. Wu, W. Song, Z. Cao, J. Zhang, A. Lim, Learning improvement heuristics for solving routing problems, *IEEE Transactions on Neural Networks and Learning Systems* 33 (9) (2022) 5057–5069.
- [28] Z. Zheng, S. Yao, G. Li, L. Han, Z. Wang, Pareto improver: Learning improvement heuristics for multi-objective route planning, *IEEE Transactions on Intelligent Transportation Systems* 25 (1) (2024) 1033–1043.
- [29] O. Vinyals, M. Fortunato, N. Jaitly, Pointer networks, in: *Proceedings of Advances in Neural Information Processing Systems*, 2015, pp. 2692–2700.
- [30] W. Kool, H. v. Hoof, M. Welling, Attention, learn to solve routing problems!, in: *the International Conference on Learning Representations*, 2019, pp. 1–25.
- [31] F. Luo, X. Li, F. Liu, Q. Zhang, Z. Wang, Neural combinatorial optimization with heavy decoder: Toward large scale generalization, in: *Proceedings of Advances in Neural Information Processing Systems*, 2023, pp. 8845–8864.
- [32] Y. Ma, J. Li, Z. Cao, W. Song, L. Zhang, Z. Chen, J. Tang, Learning to iteratively solve routing problems with dual-aspect collaborative transformer, in: *Proceedings of Advances in Neural Information Processing Systems*, 2021, pp. 11096–11107.
- [33] Y. Ma, Z. Cao, Y. M. Chee, Learning to search feasible and infeasible regions of routing problems with flexible neural k-opt, in: *Proceedings of Advances in Neural Information Processing Systems*, 2023, pp. 49555–49578.
- [34] X. Chen, Y. Tian, Learning to perform local rewriting for combinatorial optimization, in: *Proceedings of Advances in Neural Information Processing Systems*, 2019, pp. 6278–6289.
- [35] Y. Xiao, D. Wang, Z. Cao, R. Cao, X. Wu, B. Li, Y. Zhou, GELD: A unified neural model for efficiently solving traveling salesman problems across different scales, *arXiv: 2506.06634* (2025).

- [36] F. Luo, X. Lin, Y. Wu, Z. Wang, X. Tong, M. Yuan, Q. Zhang, Boosting neural combinatorial optimization for large-scale vehicle routing problems, in: the International Conference on Learning Representations, 2025, pp. 1–27.
- [37] Y. Xiao, Y. Wu, R. Cao, D. Wang, Z. Cao, X. Wu, P. Zhao, Y. Li, Y. Zhou, Y. Jiang, DGL: Dynamic global-local information aggregation for scalable vrp generalization with self-improvement learning, in: Proceedings of International Joint Conference on Artificial Intelligence, 2025, pp. 8669–8677.
- [38] H. Liang, Y. Ma, Z. Cao, T. Liu, F. Ni, Z. Li, J. Hao, SplitNet: A reinforcement learning based sequence splitting method for the minmax multiple travelling salesman problem, in: Proceedings of the AAAI Conference on Artificial Intelligence, 2023, pp. 8720–8727.
- [39] H. Gao, X. Zhou, X. Xu, Y. Lan, Y. Xiao, AMARL: An attention-based multiagent reinforcement learning approach to the min-max multiple traveling salesmen problem, *IEEE Transactions on Neural Networks and Learning Systems* 35 (7) (2024) 9758–9772.
- [40] M. Kim, J. Park, J. Park, Learning to cross exchange to solve min-max vehicle routing problems, in: the International Conference on Learning Representations, 2023, pp. 1–29.
- [41] J. Son, M. Kim, S. Choi, H. Kim, J. Park, Equity-transformer: Solving np-hard min-max routing problems as sequential generation with equity context, in: Proceedings of the AAAI Conference on Artificial Intelligence, 2024, pp. 20265–20273.
- [42] Y. Wang, Y.-H. Jia, W.-N. Chen, Y. Mei, Distance-aware attention reshaping: Enhance generalization of neural solver for large-scale vehicle routing problems, *arXiv: 2401.06979* (2024).
- [43] H. Ye, J. Wang, Z. Cao, F. Berto, C. Hua, H. KIM, J. Park, G. Song, Reevo: Large language models as hyper-heuristics with reflective evolution, in: Proceedings of Advances in Neural Information Processing Systems, 2024, pp. 43571–43608.
- [44] A. Radford, J. W. Kim, C. Hallacy, A. Ramesh, G. Goh, S. Agarwal, G. Sastry, A. Askell, P. Mishkin, J. Clark, et al., Learning transferable

- visual models from natural language supervision, in: Proceedings of the International Conference on Machine Learning, 2021, pp. 8748–8763.
- [45] Y.-D. Kwon, J. Choo, B. Kim, I. Yoon, Y. Gwon, S. Min, POMO: Policy optimization with multiple optima for reinforcement learning, in: Proceedings of Advances in Neural Information Processing Systems, 2020, pp. 21188–21198.
- [46] M. Kim, J. Park, J. Park, Sym-NCO: Leveraging symmetricity for neural combinatorial optimization, in: Proceedings of Advances in Neural Information Processing Systems, 2022, pp. 1936–1949.
- [47] R. J. Williams, Simple statistical gradient-following algorithms for connectionist reinforcement learning, *Machine Learning* 8 (1992) 229–256.
- [48] S. Karakatič, V. Podgorelec, A survey of genetic algorithms for solving multi depot vehicle routing problem, *Applied Soft Computing* 27 (2015) 519–532.
- [49] İlhan İLHAN, An improved simulated annealing algorithm with crossover operator for capacitated vehicle routing problem, *Swarm and Evolutionary Computation* 64 (2021) 100911.
- [50] J. Christiaens, G. Vanden Berghe, Slack induction by string removals for vehicle routing problems, *Transportation Science* 54 (2) (2020) 417–433.
- [51] H. Fang, Z. Song, P. Weng, Y. Ban, INViT: A generalizable routing problem solver with invariant nested view transformer, in: Proceedings of the International Conference on Machine Learning, 2024, pp. 12973–12992.